17th World Conference on Earthquake Engineering, 17WCEE

Sendai, Japan - September 13th to 18th 2020

A SELF-CENTERING ENERGY DISSIPATIVE BRACE WITH LOW PRESTRESSING

Y. Xiao[(1)], M. O. Eberhard[(2)], Y. Zhou[(3)], J. F. Stanton[(4)], J. H. Shen[(5)]

[(1)] *Doctoral student, State Key Laboratory of Disaster Reduction in Civil Engineering, Tongji University, yixiao@tongji.edu.cn; Visiting student, Department of Civil and Environmental Engineering, University of Washington, yixiaouw@uw.edu*
[(2)] *Professor, Department of Civil and Environmental Engineering, University of Washington, eberhard@uw.edu*
[(3)] *Professor, State Key Laboratory of Disaster Reduction in Civil Engineering, Tongji University (corresponding author), yingzhou@tongji.edu.cn*
[(4)] *Professor, Department of Civil and Environmental Engineering, University of Washington, stanton@uw.edu*
[(5)] *Master student, State Key Laboratory of Disaster Reduction in Civil Engineering, Tongji University, shenjhbao@tongji.edu.cn*

Abstract

A braced frame equipped with a self-centering energy dissipative (SCED) brace has been designed to limit the maximum drifts during an earthquake and to nearly eliminate residual drifts. Compared with self-centering wall structures and self-centering frame structures, a braced frame equipped with SCED braces requires only minor changes to the structural system, so it is an attractive option for the design of new and retrofitted resilient structures. The SCED braces that have been developed in the past require a high level of prestressing force, which significantly increases difficulties in component design and fabrication, and causes uncertainty in safety and long-term reliability. In addition, their energy dissipative systems have inadequate reliability or excessive complexity. This paper proposes and explores the performance of a new SCED brace that addresses these challenges. Unlike previously developed systems, the proposed system subjects the energy dissipation component to tension only. Consequently, a lower level of prestressing is required, and the dissipater does not need lateral restraint to prevent buckling, so the mild steel yielding element that is likely to have reliable long-term properties can be easily implemented. A physical configuration of the concept that implements a high strength rod-chuck ratchet system, a post-tensioned tendon system and a mild steel yielding dissipater is presented and further investigated. The paper identifies key parameters and equations that govern the brace's performance. A numerical modeling method that incorporates two user-defined materials in OpenSEES is developed and validated. Then, the new brace is compared with buckling restrained brace, conventional SCED brace and telescoping SCED brace for a one-story example industrial building. The design of the example building shows that the new brace requires less than 10% of the prestressing force required for existing SCED braces to achieve similar hysteretic relationships. The new brace also achieves 88% larger axial-elongation capacity than the conventional SCED brace, because it has lower initial strain in its prestressing tendons. The seismic performance of the braced systems equipped with the four braces are numerically investigated using the proposed modeling method for the new brace and existing approaches for the existing braces. Numerical results from the cyclic loading test show that the three SCED braces have larger post-yielding stiffness than the buckling restrained brace because of the contribution of the prestressing tendons, which remain elastic. Among the three SCED braces, the new brace has the smallest post-yielding stiffness, because it needs less amount of prestressing tendons. Numerical results from the nonlinear dynamic analyses under earthquake ground motions confirm that the braced frame equipped with the new brace would control the maximum response to about the same extent as would for existing SCED braces, while effectively eliminating residual drift, even under severe earthquakes. The new brace has a dissipater cumulative plastic deformation value of 7.4%, in relative to its length, in the worst MCE ground motions, which is small compared with the specified 22% strain capacity of the material. It is concluded that the proposed low-prestressed SCED brace successfully addresses the major challenges of previous SCED braces and it is an attractive SCED brace concept for engineering application.

Keywords: self-centering energy dissipative brace, low-level prestressing, elongation capacity, numerical investigation, system comparison

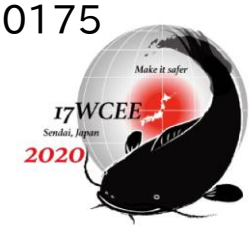

1. Introduction

Self-centering behavior is a critical feature of seismic resilient structures, because it limits the structural residual drift while controlling the maximum responses. As a result, self-centering building structures are able to achieve rapid functional recovery after an earthquake. Several self-centering structure systems have been proposed and studied, including self-centering wall structures, self-centering frame structures and braced frame structures equipped with self-centering braces. Unlike the first two systems, a braced frame equipped with self-centering braces requires only minor changes to the structures, making it an attractive candidate system for the design of new and retrofitted resilient structures [1].

To develop the new structural system, it is essential to have an effective and reliable self-centering brace. The basic concept of the self-centering energy dissipative (SCED) brace was proposed by Christopoulos et al. [2]. Generally, a SCED brace utilizes two brace components working together with a prestressing system through contacts to form a self-centering mechanism. An energy dissipater is usually incorporated to dissipate earthquake energy. However, this causes a problem, because the dissipater resists the brace to get back to its original length during unloading. To achieve a full self-centering behaviors, the prestressing force in the brace system has to be greater than the resisting force generated in the dissipater. In other words, the prestressing force needs to be greater than a half of the brace yielding strength, which is the sum of the prestressing force and the dissipater force. For example, if the brace strength is 1000 kN, a prestressing force of at least 500 kN must be applied to ensure re-centering.

The requirement for high level of prestressing force significantly limits the effectiveness and reliabilities of the SCED brace. To accommodate the large prestressing force, the SCED brace needs either a large amount of prestressing element material or a large initial strain in the material. In fact, to ensure a certain level of axial elongation capacity, an upper limit of initial strain is required, and that inevitable leads to a relatively large amounts of prestressing element material. In addition to the material usages, more prestressing element material results in larger post-yielding stiffness, because it remains elastic even after the brace yields. As a result, less hysteretic damping is generated for a given ductility.

The large prestressing force demand also leads to the following problems:

- The brace axial-elongation capacity is reduced by the relatively large initial strain in the prestressing element;
- The tendon or spring options for the prestressing system are limited to high-strength materials;
- The anchorage details are limited to those suitable for large prestressing forces;
- Safety challenges during fabrication, transportation, installation and service; and
- Large prestressing forces and stresses can lead to large, long-term prestressing losses.

Another challenge of the previously developed SCED braces is the reliability or complexity of the proposed energy dissipative systems. Most SCED braces rely on displacement-dependent friction dampers or metal yielding elements to dissipate energy. It is difficult to ensure reliable dynamic and long-term performance of friction dampers because of bolt looseness and interface corrosion. Metal yielding elements generate stable hysteretic damping and are likely to have long-term properties that are more reliable. However, lateral restraint must be provided for the yielding elements to avoid compressive buckling [3], which increases the brace complexity and adds to the cost. It is also difficult to replace the yielding element if it is surrounded by buckling-restraint materials after earthquakes.

To address these challenges, this paper proposes a new SCED brace, named Low-Prestressed Self-Centering Energy Dissipative (LP-SCED) brace. The new brace is designed to achieve full self-centering behaviors with a low level of prestressing. It can use a tension-only, metal-yielding energy dissipative mechanism that does not need lateral restraint to prevent buckling. In addition, the new brace has a larger elongation capacity than the original SCED brace due to lower initial strain. A numerical modeling method is developed and verified. Then an example braced frame building system is designed using Buckling Restrained

Brace (BRB), two previous SCED braces and the LP-SCED brace, and the four systems' component properties, axial-elongation capacity and seismic performances are compared to investigate the benefits of the new brace system.

2. Mechanism and Configuration of LP-SCED Brace

2.1 Concept and mechanism of LP-SCED brace

Fig.1 shows the schematic of the LP-SCED brace and Fig. 2 shows its flag-shape self-centering hysteretic response. The brace consists of three main components, designated as the inner component, intermediate component and outer component. The inner and intermediate components, together with a prestressing system form a self-centering mechanism, which is the same with a typical SCED brace. Here, the prestressing system uses a post-tensioned (PT) tendon system, but it can also adopt a pre-compressed disc spring system, using details such as those given by Xu et al. [4]. Unlike previously developed systems, the proposed system utilizes a tension-only energy dissipative system (the outer component), so that the resisting force from the dissipater during unloading is removed, and a low level of prestressing force in the PT tendons is sufficent to pull the sytem back to its origin length. Indeed, the outer component is constituted by a ratchet system connected in series with a dissipater. When the brace is in tension and the outer component elongates, the ratchet system is engaged and the dissipater yields to dissipate energy. When the force is reversed and the tensile force in the dissipater has been unloaded to zero, the ratchet system starts to slide and avoid compressive axial force arises in the dissipater. Once the sliding of the ratchet system and the recentering force in the PT tendons has led the system to the original length, the compressive axial force applied on the brace will be transformed by the inner and intermediate components in a tensile force acting on the outer component, which will be forced again to yield in tension.

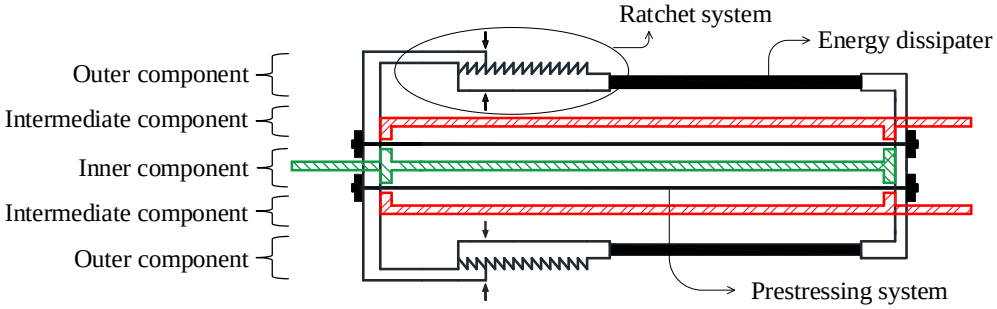

Fig. 1 – LP-SCED brace schematic

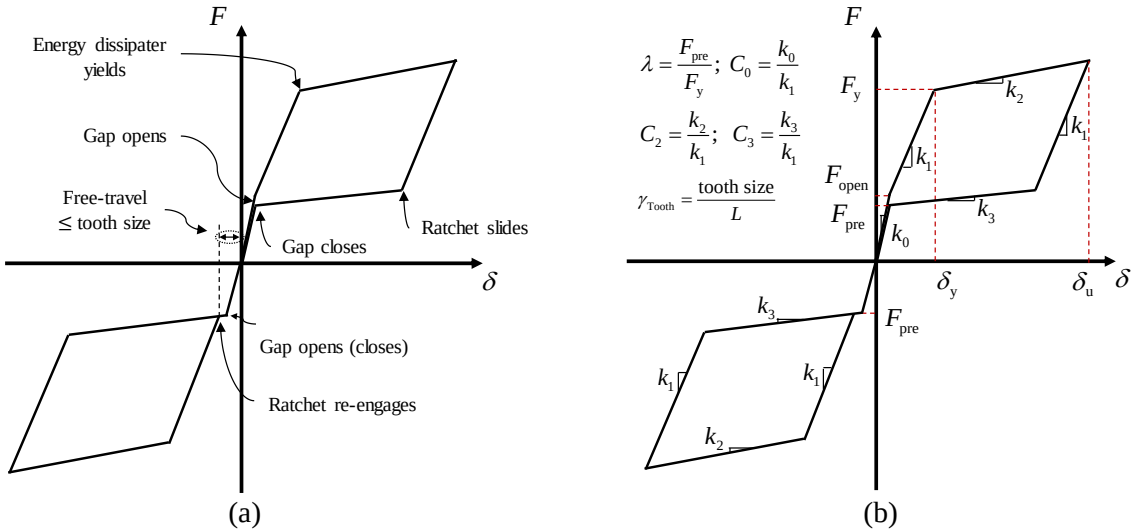

Fig. 2 – LP-SCED brace flag-shape hysteretic response: (a) brace behavior; and (b) hysteretic parameter

A number of energy dissipaters can be used alone or in combination with each other. Here, because the dissipter only subjects to tension, no lateral restraint is needed to prevent compressive buckling. Therefore, a mild steel yielding element is used, because it is reliable and economical. Because the energy dissipater is in the outer component, it can be inspected and, if needed, replaced easily after an earthquake.

2.2 Configuration of LP-SCED brace

The LP-SCED brace concept can be achieved with a number of combinations of ratchet, prestressing and dissipative systems. As an example, one physical configuraion is illustrated in Fig. 3.

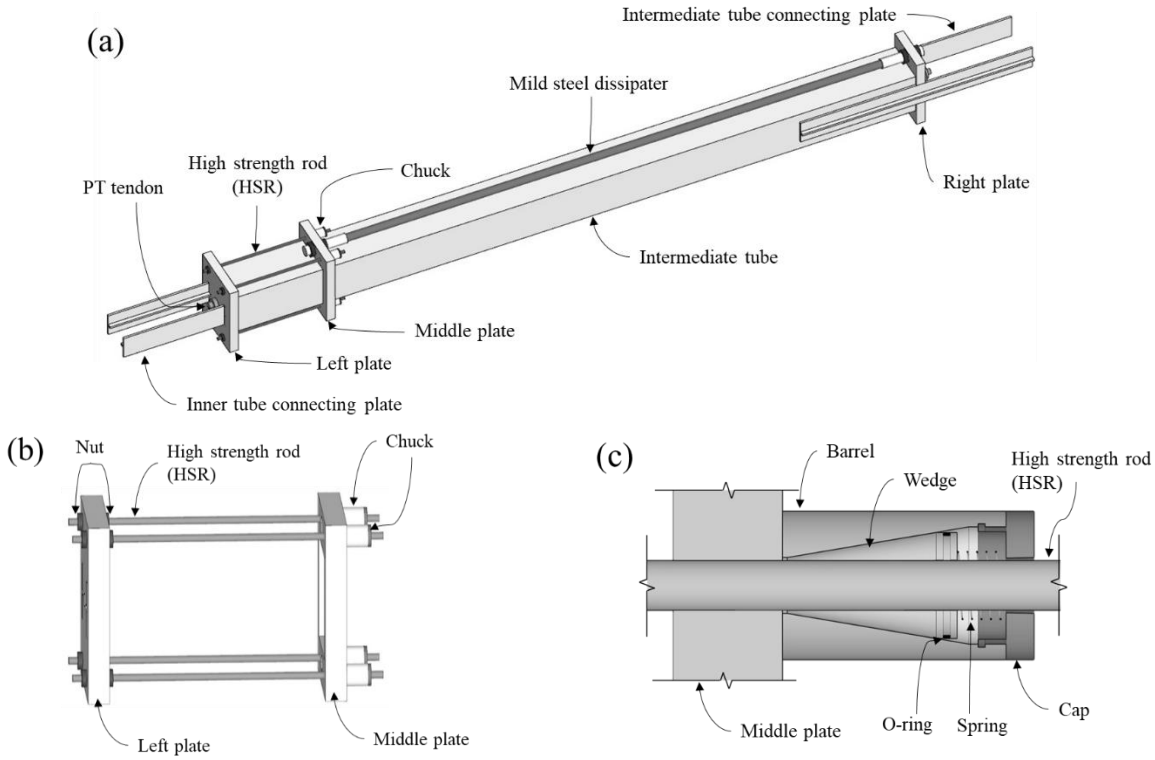

Fig. 3 – A physical configuration of LP-SCED brace: (a) brace; (b) high strength rod-chuck ratchet system; and (c) cross section of the chuck

The inner and intermediate components are designed as two rectangular tabular steel tubes with the inner tube (not shown in Fig. 3) being inserted inside the intermediate tube. For the left end of the inner tube and the right end of the intermediate tube, connecting steel plates are welded at the tubes' ends and they go through the end plates (named left plate and right plate) through slots. The PT tendons are introduced inside the inner tube and anchored on the outer side of the two end plates. Therefore, the two plates are blocking elements for the inner tube, intermediate tube and PT tendons, but they are also part of the outer component.

The physical configuration shown in Fig. 3(a) adopts a high strength rod-chuck ratchet system and mild steel dissipaters. To achieve symmetry, two dissipaters are designed and they are located to the upper and lower surfaces of the brace respectively, but only the dissipater located to the upper surface is shown in Fig. 3. The mild steel dissipaters are connected to the right plate and a middle plate using thread connection. The ratchet system is further shown in Fig. 3(b) and it consists of the left plate, the middle plate, four high strength rob (HSR), eight nuts and four chucks. The four HSRs are threaded fix connected to the left plate using the eight nuts, and connected to the middle plate through the four chucks, which are welded to the right side of the middle plate. The "chuck" refers to the commercial available anchorage hardware originally developed, fabricated and widely used in typical posttensioning systems [5]. Fig. 3(c) shows the cross section of the chuck. When the ratchet system is in tension and the HSR tends to move to the left (in relative to the chuck), the wedges will slide into the tapered interior surface so that the HSR is compressed into the barrel. In other words,

the HSR is anchored and the ratchet system is engaged. When the ratchet system is in compression and the HSR tends to move to the right (in relative to the chuck), the wedges will also slide to the right and will be out of the tapered interior surface, so the HSR can move with little resistance and the ratchet system shows a sliding behavior. Note that here the adopted high strength rod-chuck system realizes the ratchet mechanism by friction, so the ratchet tooth size as illustrated in the LP-SCED brace concept schematic (Fig. 1) is small.

3. Determining component properties from target hysteresis

Fig. 2(b) shows the parameter system that identifies the flag-shape hysteresis of the new brace. F_{open} is the brace force when the gap between inner component and the intermediate component opens. F_{pre} is the brace force when the gap closes and it is equal to the prestressing force in the PT tendons. The minor difference between F_{open} and F_{pre} is the mild steel force at the point at which the gap opens. F_y and δ_y are the brace force and deformation when the mild steel yields. δ_u is the brace axial deformation capacity. k_0~k_3 are the brace stiffness at different stages as illustrated in Fig. 2(a). In addition, four non-dimensional parameters, λ, C_0, C_2, and C_3, are further introduced as the ratio of F_{pre} to F_y, the ratio of k_0 to k_1, the ratio of k_2 to k_1, and the ratio of k_3 to k_1, respectively. Although the physical configuration shown in Fig. 3 is expected to have a small tooth size, the parameter's effect is still incorporated in the hysteretic model through γ_{Tooth} so that the model is feasible for other physical configurations. γ_{Tooth} is the length ratio of the ratchet tooth size to the brace length, L, and it affects the hysteretic model through a distance indicated as "free-travel" distance. The free-travel distance is generated because the ratchet system needs to travel for new teeth to get re-engaged each time when the outer component starts to elongate. The free-travel distance is limited by the tooth size of the ratchet.

For a targeted hysteresis shown in Fig. 2, the component properties of the brace required can be calculated by analyzing each element's behavior at each loading condition. The cross-sectional area of the PT tendon, A_{PT}, is giving as:

$$A_{PT} = C_3 k_1 \frac{\gamma_{PT} L}{E_{PT}} \tag{1}$$

where L is the length of the brace, γ_{PT} is the length ratio of the PT tendon length, L_{PT}, to L, and E_{PT} is the elastic modulus of the PT tendon material. The cross-sectional area of the mild steel, A_S, is giving as:

$$A_S = (1 - C_3) k_1 \frac{\gamma_S L}{E_S} \tag{2}$$

where γ_S is the length ratio of the mild steel dissipater length, L_S, to L, and E_S is the elastic modulus of the mild steel material. The prestressing force is calculated by definition, $F_{pre} = \lambda F_y$. The prestressing ratio, α_{pre}, which is defined by the prestressing initial stress divided by the ultimate strength, of the PT tendons can be calculated using the non-dimensional parameters:

$$\alpha_{pre} = \frac{\gamma_S \varepsilon_{S,y}}{\gamma_{PT} \varepsilon_{PT,u}^{el}} \frac{1}{C_3} \frac{\lambda}{1 - (\frac{C_0 - 1}{C_0 - 1 + C_3})\lambda} \tag{3}$$

where $\varepsilon_{S,y}$ is the yielding strain of the mild steel, and $\varepsilon_{PT,u}^{el} = \sigma_{PT,u}/E_{PT}$ is the strain corresponding to the PT tendon's ultimate strength $\sigma_{PT,u}$, assuming linear stress-strain relationship.

Once the geometry, material and component properties are determined, the axial-elongation capacity δ_u is given by:

$$\delta_u = (\varepsilon_{PT,u} - \alpha_{pre} \varepsilon_{PT,u}^{el}) \gamma_{PT} L \tag{4}$$

where $\varepsilon_{PT,u}$ is the PT tendon material ultimate strain capacity, and it equals to $\varepsilon_{PT,u}^{el}$ if the material has a linear stress-strain relationship.

4. Numerical Modeling

4.1 Model development

Fig. 4 illustrates the overall procedure of modeling the LP-SCED brace in OpenSEES, in which the new brace's characteristics are integrated into a material object ($mat5). The $mat5 material object is an assemblage of four previously defined material objects. $mat1 and $mat2 define the ratchet and dissipater (e.g. mild steel) materials respectively. $mat3 is a Series material object constructed from $mat1 and $mat2 and describes the outer component's behavior. $mat4 describes the prestressing system's (e.g. PT tendon) behavior with additional stiffness from the inner and intermediate components before the gap opens. Once $mat5 is created, it can be assigned to element objects to model the brace. Two user-defined material were developed to support the modeling method, and they are labeled in red in Fig. 4. The first material, indicated as Ratchet, was developed to model the behavior of the ratchet system; and the second material, indicated as LPSCED, was developed to simulate the tension-only behavior of the outer component ($mat3) and PT tendon ($mat4), and it was designed to construct the material object ($mat5) that describes the overall brace characteristics.

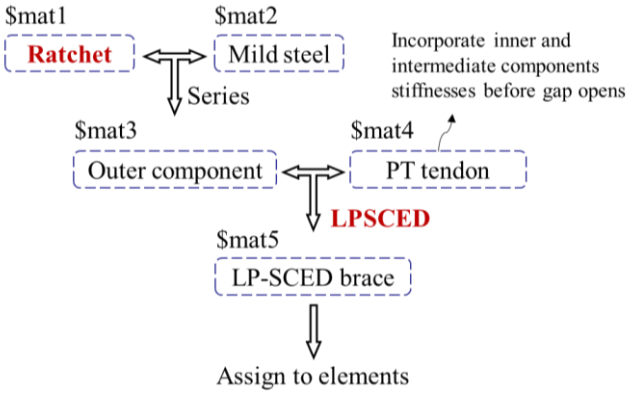

Fig. 4 – LP-SCED brace modeling method

4.2 Model validation

To validate the accuracy and numerical convergence of the proposed modeling method, a more detailed and complex analytical model was developed to simulate the behavior of each of the brace components, as shown in Fig. 5. This detailed analytical model simulates each component of the brace. The contact behavior among the three brace components are simulated using the ENT (Elastic-No Tension) Material in OpenSEES.

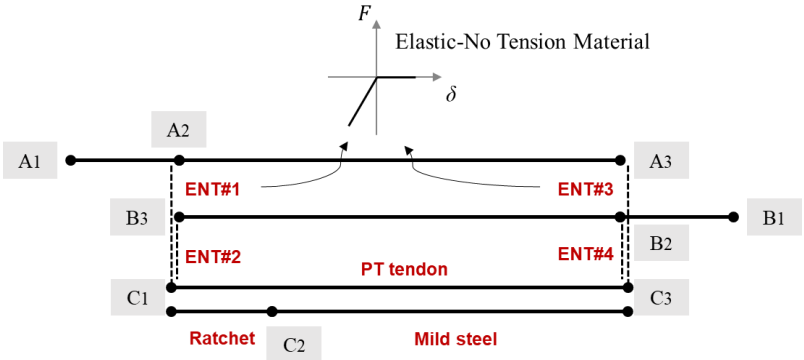

Fig. 5 – Detailed LP-SCED brace analytical model

Fig. 6 compares the computed response of the LP-SCED brace under cyclic loading, for both the proposed modeling method (Fig. 4) and the detailed analytical model (Fig. 5). In this validation simulation, the mild steel was assumed to have a bilinear constitutive model, and the PT tendon was assumed to remain in the linear-elastic range of behavior. Fig. 6 shows that the proposed modeling method generated response identical to that of the detailed model, and the ratchet system behaves as expected.

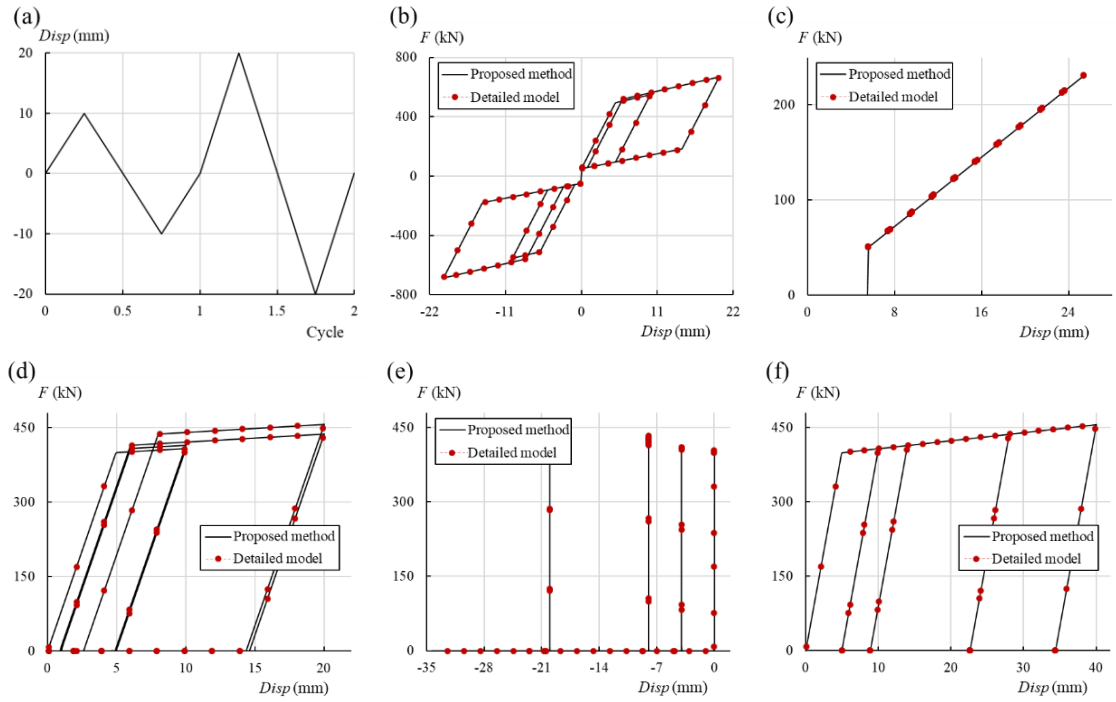

Fig. 6 – Numerical response of LP-SCED brace: (a) cyclic loading; (b) LP-SCED brace; (c) PT tendon; (d) outer component; (e) ratchet system; and (f) mild steel

5. Comparison of Example Braced-Frame Building Systems Equipped with the New and Existing Braces

5.1 Design of braced systems for example building

The plan view, elevation view and key design parameters for the example building (an industrial building) are shown in Fig. 7. The gravity load data is taken from the literature [6], and the building is assumed to be located on site class C in Seattle. The comparison of the systems will be made in the north-south direction braced frame shown in Fig. 7(b).

Four braced systems were designed to resist lateral load of the example building using the new and existing braces, which are the proposed LP-SCED brace, Buckling Restrained Brace (BRB) without prestressing, Conventional SCED (C-SCED) brace, and Telescoping SCED (T-SCED) brace. The C-SCED and T-SCED braces are previously develped self-centering braces, and their detailed mechanism and configurations can be found in Christopoulos et al. [2] and Erochko et al. [7], repectively. Fig. 8 shows the concept schematics of the C-SCED and T-SCED braces. As shown, the T-SCED brace uses two sets of PT tendons (each set represents a pair of tendons in Fig. 8) deforming in series, so that the brace elongation capacity is enhanced. These two SCED braces use friction energy dissipaters and have a typical flag-shape hysteresis which is similar with the new brace, as shown in Fig. 2.

To make it possible to compare the properties of the four brace systems consistently, it is important that the hysteretic responses of the systems be similar. The three SCED braces were designed to have the same yielding strength F_y as the BRB (=682 kN), which was designed using existing codes [8, 9]. Among the three SCED braces, their hyteretic parameter λ, which controls the height of the "flag" , were assigned to the same value (=0.05), the yielding displacement δ_y of the three SCED braces were forced to be identical as well (=13.2 mm). The C-SCED and T-SCED braces were designed to have $C_2 = C_3 = 0.05$, whereas the LP-SCED brace was designed for a lower value of $C_2 = C_3 = 0.02$ (to account for strain hardening of the mild steel). Other parameters for the LP-SCED brace include γ_{PT}=0.75, γ_S=0.625, $\gamma_{Tooth}=5\times10^{-4}$ and C_0=10. The BRB and LP-SCED braces conduct energy dissipation to a yielding mechanism, and the Q235 mild steel [10] was assumed

in the design of both the braces. The aramid fiber that is reported in Christopoulos et al. [2] and has a repeated cyclic modulus of 93 GPa and an elastic strain capacity of 2.3% was used for the PT tendons of the three SCED braces.

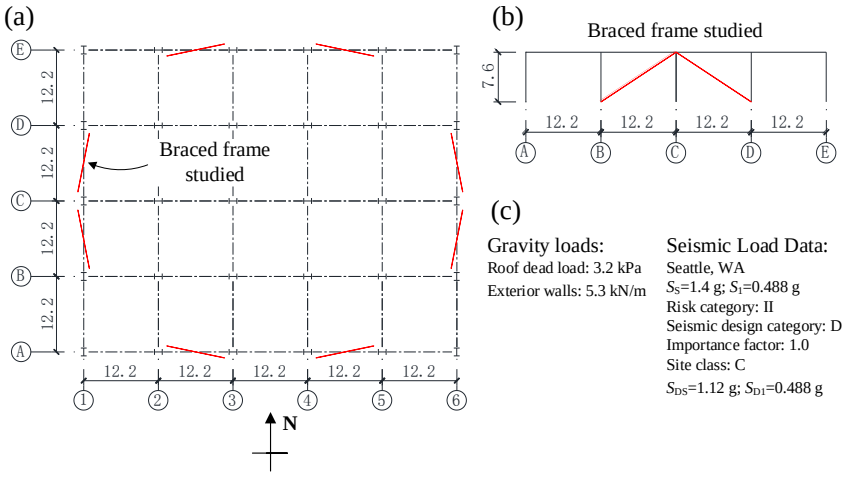

Fig. 7 – Example building: (a) plan view; (b) side elevation view; and (c) load information

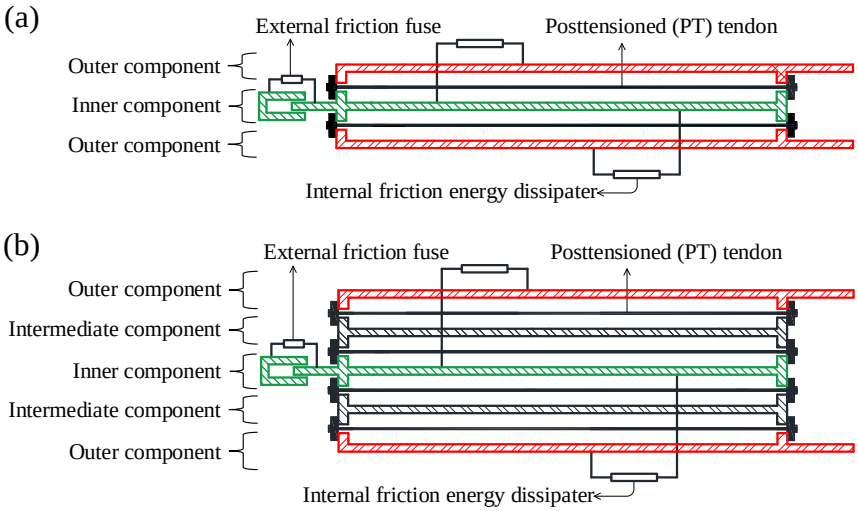

Fig. 8 – Schematics of: (a) C-SCED brace; and (b) T-SCED brace

5.2 Comparison of component properties and brace axial-elongation capacity

The properties of the key brace components, including the mild steel areas A_S, PT tendon area A_{PT}, prestressing force F_{pre} and prestressing ratio α_{pre} were calculated from the target hysteresis defined in section 5.1, and are compared in Fig. 9. The relationships between the component properties and the hysteresis of the LP-SCED brace can be found in section 3, and those of the C-SCED and T-SCED braces can be found in Christopoulos et al. [2] and Erochko et al. [8], repectively.

The BRB and LP-SCED braces use mild steel for energy dissipation, whereas the C-SCED and T-SCED braces use friction energy dissipaters. To compare the amounts of energy dissipation needed, equivalent Q235 mild steel areas were calculated for the C-SCED and T-SCED braces by $A_S=\frac{F_f}{\sigma_{s,y}}$. The three SCED braces also require prestressing components. The SCED braces all required a smaller amount of mild steel, A_S, than the BRB (Fig. 9(a)). Among the three SCED braces, the LP-SCED brace needs more mild steel, but much less PT (Fig. 9(a)). The PT tendon area, $A_{PT,}$ of the LP-SCED brace was 62% and 81% smaller than that of the C-SCED brace and of each set of tendons in the T-SCED brace, respectively. At the same time, the prestressing force

required by the LP-SCED brace was less than 10% of that needed for C-SCED brace or for each set of tendons in T-SCED brace (Fig. 9(b)). The PT tendon area A_{PT} and the prestressing force were further related using the prestressing ratio α_{pre}, which represents the used capacity of the material. This is compared in Fig. 9(c) and it is show that the PT tendons in the C-SCED and T-SCED braces used four and two times the capacity of those in the LP-SCED brace, respectively.

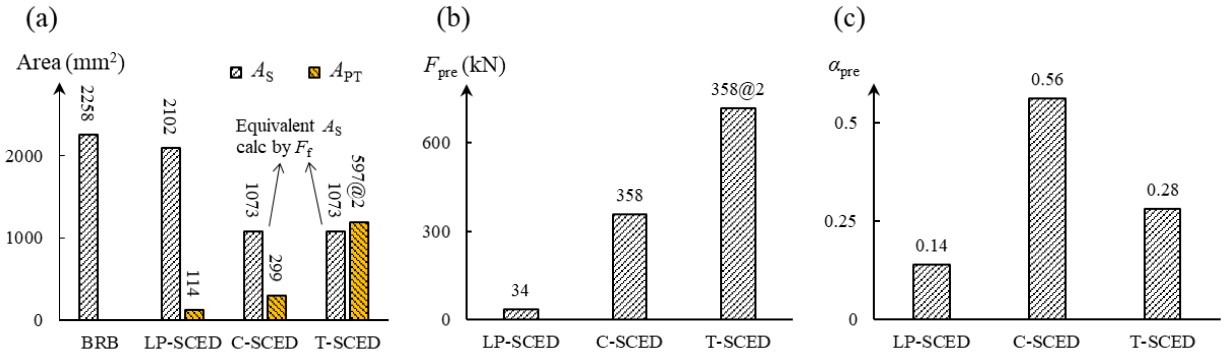

Fig. 9 – Key component properties: (a) A_S and A_{PT}; (b) F_{pre}; and (c) α_{pre}

A BRB has no physical behavior that limits axial-elongation, but the capacities of the three SCED braces can be compared at the point where the PT tendons can tolerate no further elastic extension. The brace axial-elongation capacity was calculated by dividing the axial deformation capacity δ_u over the brace length L. Eq. (4) is used to determine the δ_u for the LP-SCED brace. The equation to determine δ_u for C-SCED brace is the same with that of LP-SCED brace, whereas the δ_u of T-SCED is two times of that determined by Eq. (4), because the T-SCED has two sets of PT tendons deforming in series.

The brace axial-elongation capacity of the three SCED braces are compared in Fig. 10. Fig. 10 shows that, by adding an extra brace component and an additional set of PT tendons, the T-SCED brace increases the elongation capacity by 213% compared with that of the C-SCED brace. The LP-SCED brace, without adding an extra component and additional PT tendons, increases the elongation capacity by 88% compared with the capacity of the C-SCED brace. Referring to the example building elevation geometry (Fig. 7(b)), the allowable story drifts of the braced frame corresponding to the brace elongation capacity are calculated as 3.3%, 1.7% and 5.5% for LP-SCED, C-SCED and T-SCED systems, respectively.

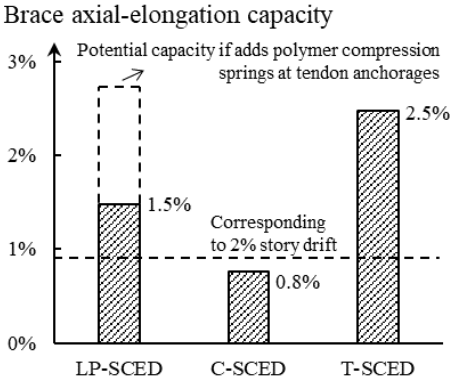

Fig. 10 – Brace axial-elongation capacity

The 1.5% elongation capacity (3.3% allowable story drift) of the LP-SCED system should be sufficient for most applications. However, if a larger story drift demand is needed, the brace elongation capacity can be further enhanced. One possible technique, which will be confirmed with experimental demonstration, is placing polymer compression springs at the PT tendon anchorages to add a source of elastic deformability in series with the tendons, as implemented in reference [11]. Because of the low level of prestressing force required by the LP-SCED brace (Fig. 9(b)), it will be easy to implement this technique in the brace by using a low-capacity springs. Creep of the compression material would be small as well.

5.3 Comparison of seismic performance

Fig. 11 shows the loading history and calculated relationships between brace elongation and brace force for cyclic loading for the four systems. The loading history was based on the Chinese code-specified quantification testing loading protocol for BRBs and has 18 cycles [12]. As intended, the four systems have the same strength and similar initial stiffnesses. But the LP-SCED, C-SCED and T-SCED systems have larger post-yielding stiffnesses (k_2) than the BRB because of the contribution of the PT tendons, which remain elastic. During the cyclic loading, both the BRB and C-SCED braces resulted in residual drift, whereas the T-SCED and LP-SCED both fully re-centered. For the BRB, residual drift is inevitable, while in the C-SCED brace, it occurred because the loading was severe and the brace exceeded it elastic capacity of 0.8%, so the external friction fuse slipping mechanism was activated to protect the tendons but results in residual drift. The hysteretic curve of the LP-SCED dissipates more energy than that of the T-SCED brace and that of the C-SCED brace before its fuse is activated, because the LP-SCED brace uses, and is capable of, a smaller post-yielding stiffness k_2, which resulted from a C_2=0.02. Therefore, for the same ductility, the LP-SCED brace dissipates more energy than the other two SCED braces.

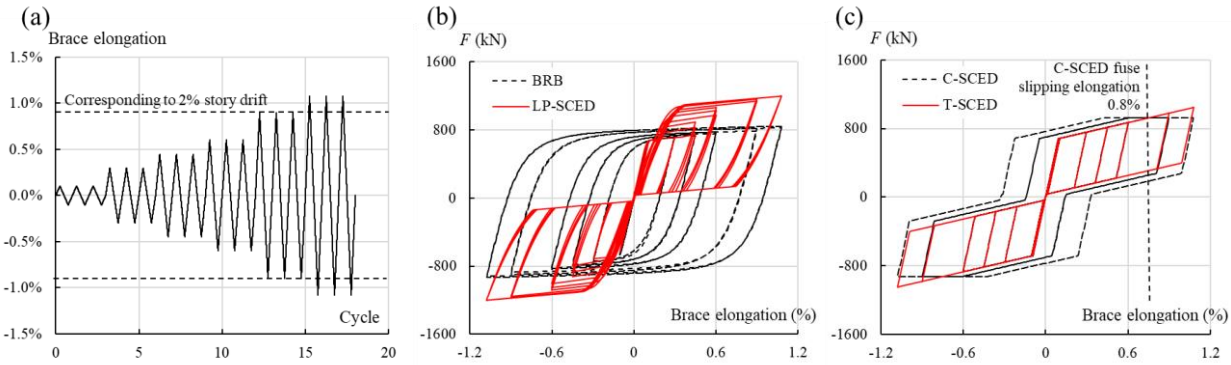

Fig. 11 – Numerical cyclic loading test: (a) loading history; (b) BRB and LPSCED responses; and (c) C-SCED and T-SCED responses

The seismic performances for earthquake ground motions of the four systems were further compared by using nonlinear dynamic analyses. The set of far-field ground motion selected by Haselton et al. [13] was used for the earthquake analyses, which includes 39 records (78 individual components). The 78 records were scaled to the design basis earthquake (DBE) level and maximum considered earthquake (MCE) level according to the acceleration spectrum value at the structural fundamental period $S_a(T_1)$ to satisfy the code-specified spectrum at the site. Note that the period of the LP-SCED system was calculated based on k_1 instead of k_0, as shown in Fig. 2(b). Fig. 12 shows the median (50%) and 84% values of the global responses of the 78 ground-motion records, including the maximum drift ratio θ_{max}, the residual drifts θ_r, and the maximum brace axial force $F_{b,max}$. The investigation of $F_{b,max}$ is of interest from the viewpoint of the forces imposed on the adjoining connections and other structural components. The 84% value corresponds to the value that was exceeded by only 16% of the records (12 out of 78). The median values are shown by the height of the bars, and the 84% values are indicated by the error bars in Fig. 12.

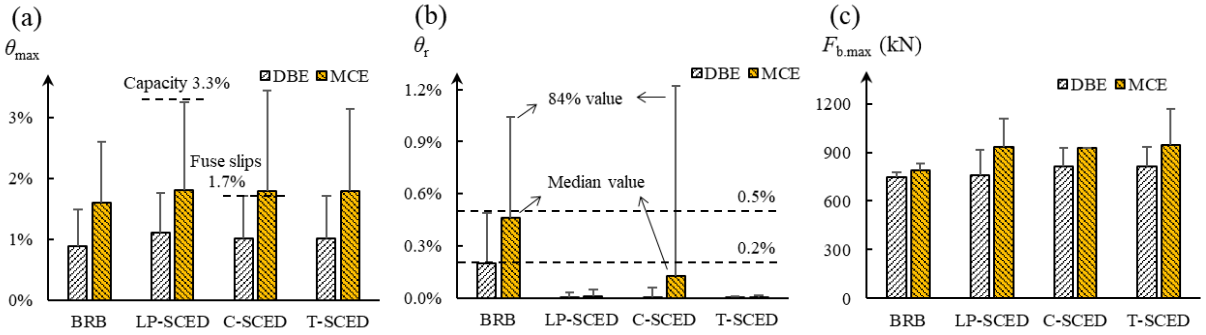

Fig. 12 –Ground motion analysis global responses (median and 84% values): (a) θ_{max}; (b) θ_r; and (c) $F_{b,max}$

Overall, the responses are dominated by the fact that the prestressing components of T-SCED and LP-SCED remain elastic and the systems always re-center, while the BRB always yields, and the C-SCED's fuse slips under severe loading, resulting in residual drift. The BRB has lower peak displacement and force, because of the higher energy dissipation and smaller post-yielding stiffness. Compared with the C-SCED and T-SCED braces, the LP-SCED brace controls the maximum response to about the extent and generates very similar maximum force demand on the adjoining connections and structural components.

5.4 Dissipater cumulative plastic deformation (*CPD*) under earthquakes

The LP-SCED brace yields only in tension, no matter what the brace loading is, and it develops and accumulates only elongations. Table 1 shows the median and 84% value of the dissipater *CPD* response under DBL and MCE from the nonlinear dynamic analyses, as well as the dissipater (Q235 mild steel for this study) nominal capacity. Under the MCE, the median *CPD* value of LP-SCED dissipater was 4.3%, and the 84% value was 7.4%. Q235 steel has a nominal elongation capacity of 22%. This is much larger than the demand, even at the MCE level, and suggests that the behavior will be satisfactory. However, the strain at fracture depends on necking, and is likely to be affected by the ratio of gage length to thickness. Depending on the detailed design of the dissipater, this may be higher than in the standard test from which the 22% capacity is measured [14], so the dissipater's elongation capacity will likely be less than that. Testing of the brace detail is needed to investigate the elongation capacity of the mild steel dissipater element. Note that the concept of the LP-SCED brace is feasible for using various dissipater materials, and if needed, a material that has sufficient elongation capacity can be applied. A different energy dissipative mechanism, in which the dissipater elongation capacity depends on component design instead of material properties, can also be adopted to eliminate the risk of dissipater fracture. For example, a typical friction damper generates friction energy dissipation through relative sliding between contacting plates. By designing a long slot for relative motion of the plates, the friction damper is capable to accommodate a large *CPD*. However, careful design of the friction damper is needed to ensure its long-term reliabilities under dynamic earthquake loading.

Table 1 Dissipater *CPD* response (in relative to dissipater length)

Seismic intensity	**Demand**		**Nominal capacity (Q235)**
	Median value	84% value	
DBL	2.2%	3.9%	22%
MCE	4.3%	7.4%	

6. Summary and Conclusions

The concept, mechanism and one physical configuration of a new low-prestressed, self-centering energy dissipative (LP-SCED) brace were presented in this paper. Governing equations that control the relationships between the component properties and the hysteresis were presented, and a modeling method for numerical simulation was developed and validated. Then, the new LP-SCED brace was compared with three existing brace systems (BRB, C-SCED, T-SCED) for a one-story example industrial building. Design result confirms that the new brace requires a low level of prestressing and has relatively large axial-elongation capacity. To achieve similar hysteretic responses (using similar materials), the LP-SCED brace only requires less than 10% of the prestressing force required for the C-SCED brace, or for each set of the PT tendons in the T-SCED brace. The LP-SCED has an axial-elongation capacity of 1.5%, which is 88% larger than that of the C-SCED brace and corresponds to 3.3% story drift. Numerical results from cyclic loading and nonlinear dynamic loading show that the LP-SCED brace generate comparable, if not better, structural control performance with the existing braces. The results were characterized by extensive yielding in the BRB and some fuse slipping in the C-SCED brace, which led to lower peak drifts for the BRB system but significant residual drifts in both systems.

The T-SCED and LP-SCED braces remained stable self-centering mechanism and re-centered under all circumstances. Their responses were similar. The LP-SCED brace has a dissipater cumulative plastic deformation value of 7.4% (in relative to its length) in the worst MCE ground motions. This is small compared with the specified 22% strain capacity of the material, and suggests that the behavior will be satisfactory. In conclusion, the proposed low-prestressed SCED brace successfully addresses the major challenges of previous SCED braces and it is an attractive SCED brace concept for engineering application. The new brace offers advantages in fabrication and service reliability compared with the C-SCED and T-SCED braces. In addition, it generates structural seismic performance that is superior to that of the BRB and the C-SCED brace, because it eliminates residual drifts, even under severe earthquakes.

7. Acknowledgements

The authors gratefully acknowledge the financial support from the National Key Research and Development Program of China (Grant No. 2016YFC0701101), the Peak Disciplinary Research Project (Grant No. 2019010107), the State Key Laboratory of Disaster Reduction in Civil Engineering Research Project of China (Grant No. SLDRCE19-B-31) and China Scholarship Council (CSC).

8. References

[1] Zhou Y, Xiao Y, Gu AQ (2019): Self-centering braced rocking frame systems and the displacement-based seismic design method. *Journal of Building Structures*, **40** (10), 17-26. (in Chinese)

[2] Christopoulos C, Tremblay R, Kim HJ, Lacerte M (2008): Self-centering energy dissipative bracing system for the seismic resistance of structures: development and validation. *Journal of Structural Engineering*, **134** (1), 96-107.

[3] Miller DJ, Fahnestock LA, Eatherton MR (2012): Development and experimental validation of a nickel–titanium shape memory alloy self-centering buckling-restrained brace. *Engineering Structures*, **40**, 288-298.

[4] Xu LH, Fan XW, Li ZX (2017): Cyclic behavior and failure mechanism of self-centering energy dissipation braces with pre-pressed combination disc springs. *Earthquake Engineering & Structural Dynamics*, **46** (7), 1065-1080.

[5] Walsh, Kevin Q, et al (2015): Effects of anchor wedge dimensional parameters on posttensioning strand performance. *PCI Journal*, **60** (3), 63-83.

[6] López WA, Sabelli R (2004): Seismic design of buckling-restrained braced frames. *Steel TIPS Report*, Structural Steel Education Council, Chicago, USA.

[7] Erochko J, Christopoulos C, Tremblay R (2014): Design and testing of an enhanced-elongation telescoping self-centering energy-dissipative brace. *Journal of Structural Engineering*, **141** (6), 04014163.

[8] ASCE 7-16 (2016): Minimum design loads for buildings and other structures. American Society of Civil Engineers, Reston, USA.

[9] AISC 341-16 (2016): Seismic provisions for structural steel buildings. American National Standards Institute, Chicago, USA.

[10] GB 50017-2017 (2017): Standards for steel structure design. China Construction Industry Press, Beijing, China.

[11] Guerrini G, Restrepo JI, Massari M, Vervelidis A (2014): Seismic behavior of posttensioned self-centering precast concrete dual-shell steel columns. *Journal of Structural Engineering*, **141** (4), 04014115.

[12] Aguaguiña M, Zhou Y, Zhou Y (2019): Loading protocols for qualification testing of BRBs considering global performance requirements. *Engineering Structures*, **189**, 440-457.

[13] Haselton CB, Liel AB, Deierlein GG, Dean BS, Chou JH (2010): Seismic collapse safety of reinforced concrete buildings. I: Assessment of ductile moment frames. *Journal of Structural Engineering*, **137** (4), 481-491.

[14] GB/T 228.1-2010 (2010): Metallic materials-tensile testing-part 1: method of test at room temperature. China Construction Industry Press, Beijing, China.

